Acta Cryst. (1987). B43, 147-159

Optical, Pyroelectric and X-ray Topographic Studies of Twin Domains and Twin Boundaries in $KLiSO_4$*

BY H. KLAPPER, TH. HAHN AND S. J. CHUNG†

Institut für Kristallographie der Technischen Hochschule, 5100 Aachen, Federal Republic of Germany

(*Received* 12 *February* 1986; *accepted* 22 *September* 1986)

Dedicated to the memory of P. P. Ewald

Abstract

Crystals of $KLiSO_4$, space group $P6_3$ at room temperature, exhibit 'twinning by merohedry' with twin laws $m\|[001]$, $2\perp[001]$ and $m\perp[001]$. This results in four kinds of twin domains which can be distinguished by the direction of electric polarity, by the rotation sense of optical activity and by X-ray topography. The arrangement of twin domains is closely related to crystal growth. Large-area twin boundaries exactly parallel to (0001), without reversal of the electric polarity (twin law $m\|[001]$), are common. Numerous thin (0001) twin lamellae with twin law $m\|[001]$ are present in the $\{10\bar{1}0\}$ prism and the $\{10\bar{1}1\}$ pyramid sectors, but not in the {0001} basal growth sectors. They originate from growth defects. Growth-sector boundaries often separate regions of opposite electric polarity according to twin law $m\perp[001]$ ('growth-sector twins'). In general, they are 'head-to-head' or 'tail-to-tail' boundaries which develop pyroelectric charges. Structural models of the twin interfaces (0001) and $(10\bar{1}0)$ show that the frequently observed large-area (0001) boundaries of twin law $m\|[001]$ are of low energy.

1. Introduction

Crystals of potassium lithium sulfate exhibit many interesting structural and physical properties which have attracted the attention of crystallographers and solid state physicists. The first publications on $KLiSO_4$ appeared at the end of the last century. Wyrouboff (1890) observed at elevated temperatures along the hexagonal optical axis a phase transition leading to a fine twinning pattern with three domain variants of optically biaxial crystals. Nacken (1907) determined the transition temperature to be 708 K. First studies of the twinning of $KLiSO_4$ were performed by Traube (1892, 1894). The strange optical interference colours of $KLiSO_4$ and their strong variation with temperature induced Blittersdorf (1929) to measure the refractive indices as a function of temperature.

The crystal structure of $KLiSO_4$ was determined by Bradley (1925). Refinements were performed by Chung (1972), who used twinned and twin-free crystals, by Karppinen, Lundgren & Liminga (1983) and by Bhakay-Tamhane, Sequeira & Chidambaram (1985*a*), using a twinned crystal. A crystal structure determination at elevated temperatures with particular attention to the thermal motion of O and Li was carried out by Schulz, Zucker & Frech (1985). Further structural investigations were published by Sandomirskii, Meshalkin & Rozhdestvenskaya (1983) and, applying neutron diffraction, by Balagurov, Savenko, Dlouha, Vratislaw & Jirak (1984).

Crystals of $KLiSO_4$ exhibit three 'main' phase transitions at 190, 708 (this is the transition detected in 1890 by Wyrouboff) and 950 K. In addition, at least two further transitions have been found, but the results are not consistent. Since 1979 many papers on the physical properties and phase transitions of $KLiSO_4$ have been published. A short and comprehensive survey is given by Schulz, Zucker & Frech (1985). More recent publications are the study of the thermal anomalies in the temperature range 573-1073 K (Kassem, El-Wahidy, Kandil & El-Gamal, 1984), the Brillouin study of the 708 K transition (Young, Katiyar & Scott, 1984), the Raman scattering investigation of the orientational phase transition at 201 K (Bansal & Roy, 1984), the X-ray and the neutron study of the low-temperature phase transitions (X-rays: Tomaszewski & Lukasziewicz, 1983; neutrons: Bhakay-Tamhane, Sequeira & Chidambaram, 1985*b*) and the investigation of the ferroelasticity and the domain pattern in the phase below 190 K (Cach, Tomaszewski & Bornarel, 1985; Cach, Tomaszewski, Bastie & Bornarel, 1984; Krajewski, Breczewski, Kassem & Mróz, 1984; Zeks, Lavrencic & Blinc, 1984; Balagurov, Savenko, Dlouha, Vratislaw & Jirak, 1984). Incommensurate phases have, with controversial results, been reported by Fonseca, Ribeiro, Gazzinelli & Chaves (1983) and

* This paper should be regarded as forming part of the Ewald Memorial Issue of *Acta Cryst.* Section A published in November 1986.

† Present address: Department of Ceramic Engineering, College of Engineering, Seoul National University, Seoul, Korea.

0108-7681/87/020147-13$01.50

© 1987 International Union of Crystallography

by Li (1984). The effect of hydrostatic pressure on the phase transitions of $KLiSO_4$ has been investigated by Fujimoto, Yasuda & Hibino (1984). Inelastic neutron scattering experiments on room- and low-temperature phases have been carried out by Eckold & Hahn (1987). Further studies of phase transitions and physical properties of $KLiSO_4$ are reported by Abello (1985), Maezawa, Takeuchi & Ohi (1985), Ivanov (1985), Krajewski, Breczewski, Piskanowicz & Mróz (1985), and Fujimoto, Yasuda & Hibino (1985*a*,*b*).

The room-temperature structure of $KLiSO_4$ and several related compounds (*e.g.* $KLiBeF_4$, $RbLiBeF_4$) (Bradley, 1925; Hahn, Lohre & Chung, 1969, 1970; Chung & Hahn, 1972*a*,*b*; Hahn & Chung, 1973) are distorted stuffed derivatives (space group $P6_3$) of the ideal hexagonal tridymite framework (Buerger, 1954). The SO_4 and LiO_4 tetrahedra form an ordered array in which the apices of the two types of tetrahedra point in opposite directions along the hexagonal axis, thus leading to a polar (pyroelectric) structure. The large K ions are 'stuffed' into the channels of the framework. Structural views are given in Figs. 10–12. These compounds show a strong tendency to develop 'twinning by merohedry' (*cf.* Donnay & Donnay, 1974; Catti & Ferraris, 1976; Hahn, 1981). Here a symmetry element, which is contained in the point-symmetry of the lattice (holohedry) but not of the crystal, acts as a twin element. Twin domains of this type have the same lattice in parallel orientation, *i.e.* the reciprocal lattices coincide. Two types, I and II, of twinning by merohedry must be distinguished (Catti & Ferraris, 1976).

Type I. The twin element is contained in the Laue symmetry of the crystal. This type can always be considered as an inversion twin. The Laue classes and the diffraction intensities of twinned and single crystals are the same, *i.e.* the structure determination is not hampered.

Type II. The twin element does not belong to the Laue symmetry of the crystal but is contained in the lattice symmetry (holohedry). If both domain variants occur with the same volume, the Laue class of the twinned crystal appears as a supergroup of index 2 of the Laue class of the single crystal. Difficulties are usually encountered in structure determination, owing to changes in diffraction intensities. Certain sets of reflections, however, are not affected by the twinning, like $h0\bar{h}l$ and $hh\bar{2}\bar{h}l$ for $KLiSO_4$.

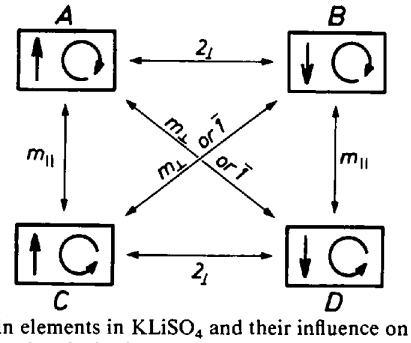

Fig. 1. Twin elements in $KLiSO_4$ and their influence on the direction of the electrical axis and the sense of optical activity. Straight arrows: direction of electrical axis. Circular arrows: sense of optical rotation. Rectangles *A*, *B*, *C*, *D* represent the four possible types of twin domains.

Generally, in twinning by merohedry, the maximal number of domain variants is equal to the index of the point group of the crystal with respect to the holohedry; possible values of the index are 2, 4 and 8.

The point group 6 of $KLiSO_4$ is a polar subgroup of index 4 of its lattice symmetry $\frac{6}{m}\frac{2}{m}\frac{2}{m}$. This compound exhibits a right- and a left-handed structure and in each the polar axis can point upwards or downwards, giving rise to three laws and four domain variants which can be distinguished by means of optical and electrical observations. This is schematically illustrated in Fig. 1. If the twin domains are submicroscopically small and have equal volumes, one or both physical effects are cancelled, depending on the twin element(s) present. The twin laws, the effect of twinning on optical activity and electrical properties and the apparent symmetry of submicroscopically twinned crystals are set out in Table 1. These twin laws were found by Traube (1892, 1894) in a study of the symmetry of etch pits and of pyroelectric decoration patterns. The purpose of the present paper is the investigation of the following aspects of twinning in $KLiSO_4$:

(i) Characterization of the four domain variants by combination of optical and electrical methods and X-ray topography.

(ii) Shape and arrangement of twin domains in relation to crystal growth and growth defects (*e.g.* dislocations).

(iii) Structural models of twin interface and their correlation with observed boundaries.

2. Experimental procedures

2.1. *Growth and preparation*

The $KLiSO_4$ starting material was synthesized by dissolving equimolar amounts of pure K_2SO_4 and $Li_2SO_4.H_2O$ in distilled water and by evaporating at 333 K. Large single crystals of dimensions up to 6 cm (duration of growth: 6–12 weeks) were grown from aqueous solutions by slow evaporation of the solvent at 323 K. They exhibit growth faces $\{\bar{1}011\}$, $\{10\bar{1}0\}$ and $\{0001\}$. Under these growth conditions the faces $\{10\bar{1}1\}$ and $\{10\bar{1}\bar{1}\}$ have the slowest growth velocity.*

* Because the crystals are of crystal class 6 the non-equivalent pyramids $\{10\bar{1}1\}$ and $\{10\bar{1}\bar{1}\}$, as well as the pedions (0001) and $(000\bar{1})$, should occur with different morphological significance. Due to twinning, however, the two pyramids and the two pedions show equal development, thus simulating a bipyramid and a pinacoid with morphological symmetry $6/mmm$.

Table 1. *Twinning by merohedry and its influence on physical properties and symmetry of* $KLiSO_4$ *(crystal class 6)*

Twin element	Abbreviated symbol	Twin type	Sense of optical rotation	Sign of pyro- and piezoelectric effect	Apparent symmetry of submicroscopically twinned crystal (equal volume of domains)	Apparent Laue class of submicroscopically twinned crystal (equal volume of domains)
$m\perp[001]$ or $\bar{1}$*	$m_\perp$	I	reversed	reversed	$6/m$	$6/m$
$m\parallel[001]$ in $\{10\bar{1}0\}$ or in $\{11\bar{2}0\}$	$m_\parallel$	II	reversed	unchanged	$6mm$	$6/mmm$
$2\parallel\langle 100\rangle$ or $\langle 210\rangle$	$2_\perp$	II	unchanged	reversed	622	$6/mmm$
Simultaneous presence of all three twin elements (four domains)	—	—	—	—	$6/mmm$	$6/mmm$

* Twin elements $m\perp[001]$ and $\bar{1}$ are equivalent because m is perpendicular to an even-fold axis.

The corresponding growth sectors frequently contain small inclusions of liquid which are arranged in layers parallel to the growth face and therefore have a milky appearance. The $\{10\bar{1}0\}$ and $\{0001\}$ growth sectors, on the other hand, are optically clear. By using large seed plates cut parallel to $(10\bar{1}0)$ and (0001), crystals with large and clear $\{10\bar{1}0\}$ and $\{0001\}$ growth sectors were obtained. Plates parallel to $(10\bar{1}0)$, (0001) and $(11\bar{2}0)$ with a thickness between 0.6 and 1.5 mm were cut with a string saw and water as solvent. The plates were flattened and polished on a wet soft cloth.

2.2. *Optical observations*

The optical activity of $KLiSO_4$ and its changes due to twinning are most clearly observed along the optical axis [001]. The specific rotatory power for this direction and for yellow light ($\lambda = 578$ nm) is $\rho = 4{\cdot}3°\,mm^{-1}$. In this investigation (0001) plates were illuminated with polarized light and observed through a rotatable analyser. The domains with optical rotation were detected by different extinction positions of the analyser. In regions of overlapping twin domains the relative portions of both twins can be determined by the deviation of the rotation angle from its maximum value ρd (d = thickness of crystal plate) for the untwinned crystal.

Optical domains associated with twin laws $m_\parallel$ and $m_\perp$ were also observed in $(10\bar{1}0)$ plates with the light propagating perpendicular to the optical axes (Fig. 2*b*). The difference of brightness in different domains is strongest when polarizer and analyser deviate by 3-5° from the crossed position and when the plate is aligned close to the extinction position. It is known that optical activity can occur also in the case of light propagation perpendicular to the optical axis (Scivessy, 1928; Born, 1933). The observation of this effect in $KLiSO_4$, however, is rather surprising, since the optical activity for this direction is usually too small to be detected owing to the dominating effect of birefringence. $KLiSO_4$, however, has a very small birefringence: it is $\Delta n = 0.0006$ for yellow light (Blittersdorf, 1929) and thus about 20 times smaller than the (already small) birefringence of quartz. This may be the explanation for the strong visibility of the domains in Fig. 2(*b*). The final interpretation of this phenomenon is postponed to a more precise study of the optical properties of $KLiSO_4$. Consequently, in this paper no conclusions about the twin laws were drawn from observations of optical domains in $(10\bar{1}0)$ plates.

2.3. *Pyroelectric investigations*

In order to observe domains with opposite electrical polarity directly, heated or cooled crystals were decorated with charged particles. In the old method of Kundt (1883) the crystal is sprayed with sulfur and meninge powder. The yellow sulfur particles deposit on the positively and the red meninge particles deposit on the negatively charged surface regions. This method suffers from a lack of spatial resolution. Very small twin domains cannot be resolved and the densely twinned regions appear uncharged.

In order to obtain higher spatial resolution of the pyroelectric decoration the method of Bury & McLaren (1969) was employed in which a developer for copying automats is applied. In this study the developer Nashua 1220 (copygraph) was used. It is a suspension of very fine negatively charged black particles in a highly insulating organic liquid. Pyroelectric decoration is performed by dipping the crystal plate for about 10 s into the hot (323-333 K) or cool (273 K) developer. During this period the temperature of the crystal is increased or decreased and pyroelectric charges are formed. The positively charged domains become covered by the black developer particles whereas the negative regions remain clear (*in situ* decoration).

By this method electrical domains in (0001) as well as in $(10\bar{1}0)$ or $(11\bar{2}0)$ plates can easily be detected. For (0001) plates the positive and negative pyroelectric charges are formed over the whole (0001) surface of the domains (domain decoration). The $(10\bar{1}0)$ and

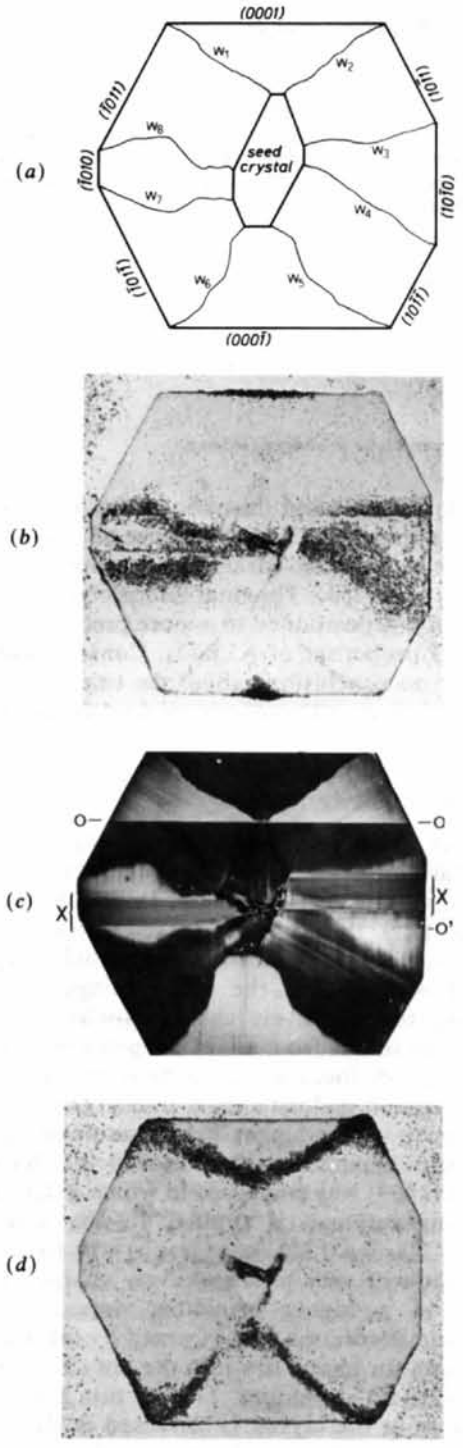

Fig. 2. Plate parallel to $(1\bar{2}10)$, about 0.6 mm thick, horizontal dimension 12 mm. (*a*) Position of the seed crystal and arrangement of growth sectors in the plate. The labels W_1–W_8 mark the boundaries between different growth sectors. (*b*) Plate between polarizers with ≈4° deviation from the crossed position. The axis [001] is rotated by ≈2° with respect to the vertical polarizer direction. In this arrangement maximum contrast of optical domains was observed. Photograph in white light. (*c*) Pyroelectric decoration (sulfur only) during heating. (*d*) Pyroelectric decoration during cooling.

$(11\bar{2}0)$ surfaces, however, remain free of charges because they are parallel to the electrical axis. Charges occur only at 'head-to-head' or 'tail-to-tail' boundaries between domains of opposite polarity (boundary decoration). In general terms, plates cut parallel to the electrical axis show only boundary decoration, whereas plates cut perpendicular or inclined to the axis exhibit domain decoration.

Electrical twinning can also be investigated by means of the longitudinal piezoelectric effect parallel to [001]. In order to detect small twin domains, the surface of a (0001) plate should be examined pointwise with a small piston. This procedure, however, is rather tedious and does not give more information than the simpler pyroelectric investigation.

2.4. *X-ray topography*

X-ray topography is a valuable method for revealing twinning of type II (see *Introduction*). The different domains in one specimen can be displayed by using pairs of reflections *hkl* and *h'k'l'* which are non-equivalent in the single crystal but are related by the twin element, *i.e.* the two reflections must be symmetrically equivalent in the holohedry but not in the Laue class of the crystal. Accordingly, their structure factors are different. If in a topograph a twin domain *A* is imaged by reflection *hkl* with intensity F^2, domain *B* reflects with different intensity $F'^2 \neq F^2$. The twin regions *A* and *B*, therefore, are visible by domain contrast. If the crystal is imaged by reflection *h'k'l'* of domain *A*, the intensities of *A* and *B* are reversed.

In the Laue class $6/m$ of $KLiSO_4$ reflections *hkil* and *khil* with $h \neq k$, $h \neq 0$, $k \neq 0$ belong to the above category. They are not equivalent in $6/m$ but are related if twin elements $m_{\parallel}$ or $2_{\perp}$ of type II are present. The difference in structure factor is maximal for the pair $12\bar{3}0$ and $21\bar{3}0$ (Chung, 1972):

$$F(12\bar{3}0) = 1{\cdot}6, \quad F(21\bar{3}0) = 18{\cdot}2.$$

The striking domain contrast for this pair of reflections is apparent in some of the following topographs (*cf.* Figs. 3*a*, *b*). The intensities of reflections $hh\overline{2h}l$, $h0\bar{h}l$, and $000l$ are not influenced by twinning. These reflections are therefore suitable for X-ray topographic investigations of other defects like dislocations (*cf.* Figs. 3*c*, *d*).

It should be noted that this kind of domain contrast has also been applied to image Dauphiné twin domains in quartz (McLaren & Phakey, 1969; Lang, 1965, 1967). Dauphiné twin domains can, for example, be distinguished X-ray topographically by using reflections of the pair $10\bar{1}0$ and $10\bar{1}\bar{1}$. An extreme contrast of Dauphiné domains, similar to that of Figs. 3(*a*) and 3(*b*), occurs if reflections of the pair $30\bar{3}1$ (very strong) and $30\bar{3}\bar{1}$ (weak) are used (Lang, 1965).

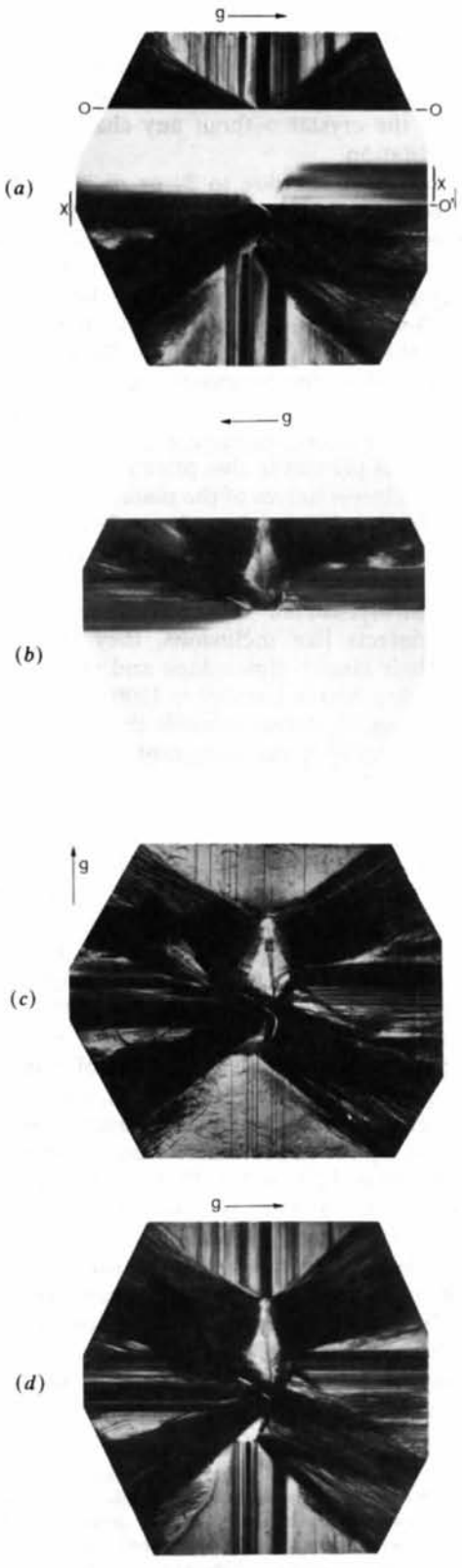

Fig. 3. X-ray topographs of the plate of Fig. 2 ($\lambda = 0.709$ Å). (*a*) Reflection $21\bar{3}0$, (*b*) reflection $12\bar{3}0$, (*c*) reflection 0004, (*d*) reflection $30\bar{3}0$. The diffraction vectors are indicated by arrows.

Table 2. *Detection of twin laws by optical activity, pyroelectricity and X-ray topographic domain contrast*

Twin law	$2\perp[001]$ (type II)	$m\parallel[001]$ (type II)	$m\perp[001]$ (type I)
Optical activity	no	yes	yes
Pyroelectricity	yes	no	yes
X-ray topography	yes	yes	no

Twinning of type I cannot be detected by domain contrast because the twin element always relates two reflections of a Friedel pair which have the same intensity, except when anomalous scattering is appreciable. In $KLiSO_4$, therefore, domains related by the twin law $m_\perp$ (or $\bar{1}$) cannot be distinguished by X-ray topography.

The X-ray topographic studies in this paper were performed using the method of Lang (1959). All topographs were taken with Mo $K\alpha_1$ radiation, for which $KLiSO_4$ has a linear absorption coefficient $\mu_0 = 17\ cm^{-1}$.

In Table 2 the possibilities of detecting the various twin elements of $KLiSO_4$ by the three methods described above are summarized. It is apparent that in all cases two methods are sufficient to determine the twin law.

3. Results

In this section the main features of twinning and of dislocations in $KLiSO_4$ are described. The interpretation of the numerous observations is given in § 4.

3.1. *Twinning*

Figs. 2 and 3 show the optical, pyroelectric and X-ray topographic observations of twin domains and twin boundaries in a plate cut parallel to $(1\bar{2}10)$, which contains part of the seed crystal. The location of the seed crystal and the arrangement of growth sectors with their boundaries are illustrated in Fig. 2(*a*).

The optical domains (Fig. 2*b*) are identical to the growth sectors. In addition, an optical boundary *O*–*O* and groups of narrow twin lamellae *X* parallel to (0001) are observed in the $\{10\bar{1}0\}$ growth sectors. The pyroelectric decorations (Figs. 2*c*, *d*) demonstrate that a reversal of the electric polarity occurs at the growth sector boundaries $W_1, W_2, \ldots, W_8$. No decoration appears at *O*–*O*, which is obviously a boundary without a reversal of the electric polarity. In Fig. 2(*c*) the 'head-to-head' and in Fig. 2(*d*) the 'tail-to-tail' boundaries are decorated. The bundles *X* of twin lamellae contain a few (about ten) boundaries with a reversal of the electric axis. These boundaries cannot be detected by the decoration with sulfur powder (except for the one boundary marked by an arrow in Fig. 2*c*), but are clearly resolved by the copygraph developer method.

The X-ray topographs in Figs. 3(*a*), (*b*) (reflections $21\bar{3}0$ and $12\bar{3}0$) of the same plate reveal twin domains related by twin laws of type II ($m\|[001]$ or $2\perp[001]$). The boundaries *O-O* and *O'* as well as the lamellae *X* are visible by domain contrast. Because the thickness of the majority of lamellae is less than the topographic resolution (about 3 μm), these bundles appear in both reflections (Figs. 3*a*, *b*) with medium intensity.

The other intensity contrasts in Figs. 3(*a*), (*b*) are not related to twinning. They are mainly due to dislocations which occur in the various growth sectors with highly different density. This is evident from Figs. 3(*c*) and 3(*d*) which show topographs with reflections 0004 and $30\bar{3}0$. These reflections cannot reveal twinning as explained in § 2.4. The contrast variations between Figs. 3(*c*) and 3(*d*) are due to the specific character of the dislocations (*cf.* § 3.2).

Combining the observations in Figs. 2 and 3 the various twin boundaries can be attributed to the twin laws as follows (*cf.* Table 2). The growth-sector boundaries W_1-W_8 separate regions of opposite electric polarity which show no X-ray domain contrast. Thus the twin law is $m\perp[001]$ (type I). The twin boundaries *O-O*, *O'* and the majority of boundaries between the lamellae *X*, however, separate domains of the same electric polarity and of strong domain contrast. The twin law is $m_\|$ (type II).

On the basis of these results the various twin domains can be identified in terms of the domain types of Fig. 1. This is shown in Fig. 4 which demonstrates that the four possible domain types and the three twin laws are present.

The following geometrical features of the '$m_\|$ boundaries' are noteworthy. All these boundaries extend from the seed to the surface of the crystal and are exactly parallel to (0001). No steps are visible within the limit of optical and X-ray topographic resolution. This is an indication of a low-energy interface (*cf.* § 4.2). The twin boundary *O-O* coincides exactly with the small (0001) facet of the seed crystal. This boundary was nucleated at the beginning of growth, obviously by the same defects (inclusions) which are

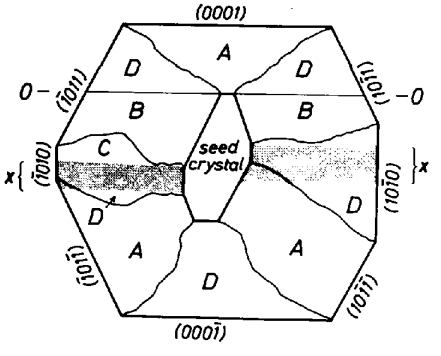

Fig. 4. Types *A*, *B*, *C*, *D* of twin domains (Fig. 1) in the plate of Figs. 2 and 3.

the origin of a bundle of grown-in edge dislocations parallel to [001] (Figs. 3*c* and 3*d*). The twin lamellae in the left prism sector $(\bar{1}010)$ and the boundary *O'* were already present in the seed crystal. They have grown with the crystal without any change in their (0001) orientation.

In $KLiSO_4$ twinning due to $2_\perp$ or $m_\|$ (type II) is observed only in $\{10\bar{1}1\}$ and $\{10\bar{1}0\}$ growth sectors. This is demonstrated in Fig. 5 which shows the distribution of twin lamellae in a $(1\bar{2}10)$ plate. It was cut from a crystal which was grown on a large (0001) seed plate. Twin lamellae appear only within the seed plate and in the $\{10\bar{1}1\}$ growth regions. They originate from the growth-sector boundaries and from small liquid inclusions. They are not revealed by pyroelectric decoration. The twin element is $m_\|$. Twin element $m_\perp$, however, is present in this plate too because the upper and the lower halves of the plate have opposite polarity. The border between both 180° domains extends along one surface of the seed crystal from *S* to *S'*.*

Because the $m_\|$ twin lamellae in Fig. 5 are nucleated at growth defects like inclusions, they should be limited in their lateral dimensions and should have the form of thin bands parallel to (0001), extending from the nucleating defect towards the growth face. This is confirmed by X-ray topographs of plates with other orientations and locations and by optical and pyroelectric observations (*cf.* Fig. 7).

In some regions of Fig. 5 the twinning is so fine and dense that the twin bands cannot be resolved by X-ray topography. The highest density of lamellae generally occurs in the $\{10\bar{1}0\}$ prism sectors. This is demonstrated by the topographs of Figs. 6(*b*) and 6(*c*) obtained from a $(1\bar{2}10)$ plate. In contrast to Fig. 5 with a (0001) seed, in Fig. 6 a large $(10\bar{1}0)$ plate cut from a twin-free (0001) growth sector was used as seed crystal. Although the seed is free of twinning, the $\{10\bar{1}0\}$ growth regions are densely $m_\|$-twinned by (0001) lamellae, as indicated by the striated horizontal contrasts and by the approximately equal intensities in both reflections $12\bar{3}0$ and $21\bar{3}0$. In addition, a few (0001) boundaries of twin law $m_\perp$ or $2_\perp$ occur, as revealed by pyroelectric decoration.

In such densely twinned regions the symmetry appears to be higher than in untwinned areas (*cf.* Table 1). In fact, X-ray precession photographs of the seed region of Fig. 5 revealed Laue class $6/m$, whereas in the $(10\bar{1}0)$ growth sectors of the same crystal Laue class $6/mmm$ was observed.

* Inside the {0001} sectors of Fig. 5 no twinning according to $m_\perp$ is present. Some other crystals, however, exhibit neither optical activity nor pyroelectricity in these sectors, demonstrating the presence of fine twinning $m_\perp$. This is confirmed by X-ray topography. These regions are strongly disturbed, as indicated by the roughness of the (0001) growth faces, by optical inhomogeneities, by strong kinematical topographic contrasts, and by the tendency to form cracks.

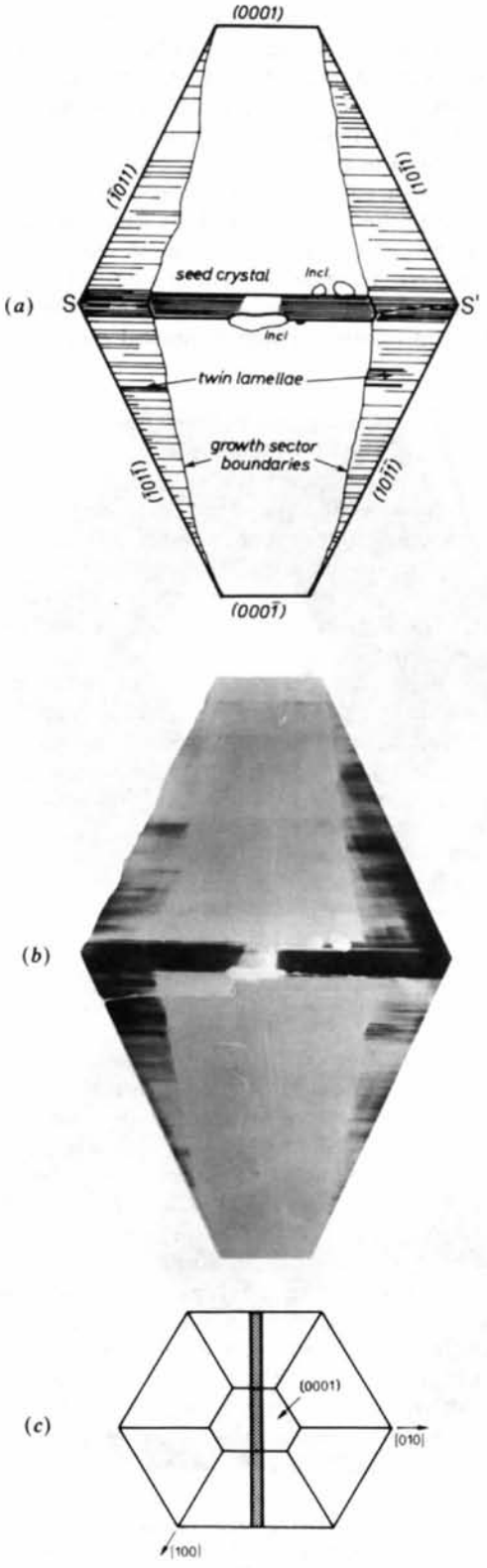

Fig. 5. Plate parallel to (1$\bar{2}$10), approximately 1 mm thick, horizontal dimension 22 mm. (*a*) X-ray topograph in reflection 12$\bar{3}$0, (*b*) geometry of growth sectors and distribution of twin lamellae, (*c*) position of the plate in the original crystal.

Figs. 7 and 8 present light photographs and pyroelectric decoration patterns of two (0001) plates prepared from one crystal. The plate of Fig. 7 was cut through the seed crystal, the contours of which are clearly visible in the centre, and contains regions grown on prism faces. Many of the striated contrasts radiating from the seed crystal are caused by local inversion or reduction of the optical rotation due to the presence of twin lamellae.

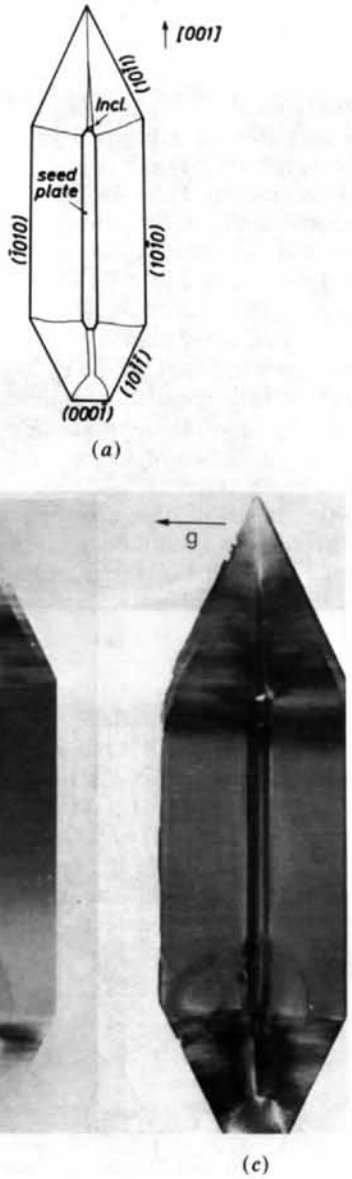

Fig. 6. Plate parallel to (1$\bar{2}$10), approximately 1 mm thick, cut from a crystal grown on a large untwinned (10$\bar{1}$0) seed plate. Horizontal dimension 11 mm. (*a*) arrangement of seed plate and growth sectors, (*b*) X-ray topograph in reflection 21$\bar{3}$0, (*c*) X-ray topograph in reflection 12$\bar{3}$0. The dark line contrasts in the seed plate in (*c*) are grown-in dislocations parallel to [001]. The horizontal striated contrasts are much better resolved in the original topographs.

The plate of Fig. 8 consists of dark outer growth regions $\{10\bar{1}1\}$ and an inner (0001) sector. The difference in transmitted light between the outer and the inner part is due to an inversion of the sense of optical rotation. Pyroelectric decoration (Fig. 8*b*) reveals opposite electric polarity between the inner and the outer sectors. Thus this twinning is due to $m_\perp$. It corresponds to the 'growth-sector twinning' in the top and the bottom parts of Figs. 2(*b*) and 2(*d*).

Many details of the optical images (twin bands *T*, growth striations *S* and line contrasts *L*) are also visible in the pyroelectric decoration patterns. It is an interesting feature that in the specimen of Fig. 7 striations *S* parallel to the growth faces occur which have the typical appearance of growth striae. These growth striations which are generally due to variations in impurity content are here accompanied by changes of optical rotation and pyroelectric charges. Thus they seem to be caused by $m_\perp$-twinning. They obviously correspond to the vertical striations which are faintly visible in the $\{10\bar{1}0\}$ and $\{10\bar{1}1\}$ growth sectors of Fig. 2(*b*). These striations are not sharply bounded, as are the $m_\parallel$ twin lamellae parallel to (0001), and they exhibit a continuous change of optical rotation. The

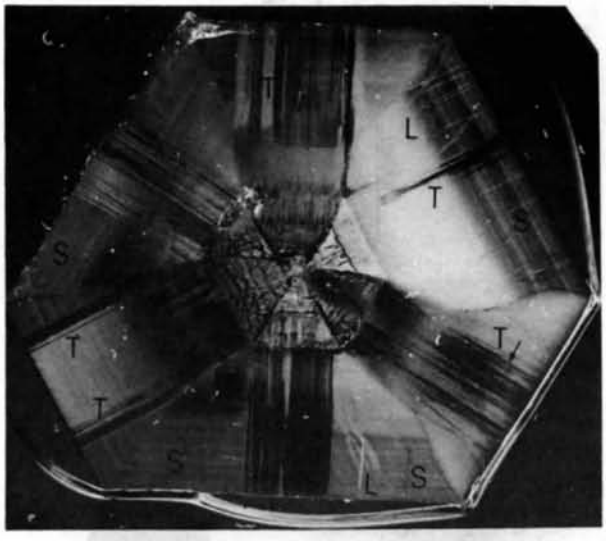

(*a*)

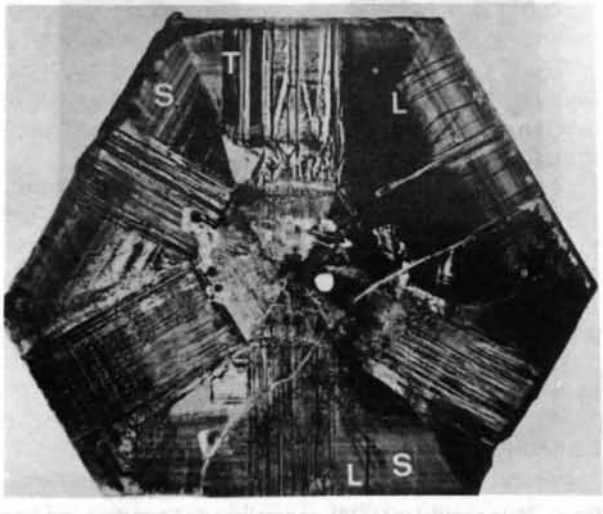

(*b*)

Fig. 7. Plate parallel to (0001) cut through the seed crystal. Thickness ≃1 mm, horizontal dimension 12 mm. It consists mainly of regions grown on prism faces. (*a*) Optical photograph of the plate between crossed polarizers. (*b*) pyroelectric decoration pattern. Only one side of the plate is decorated. *T* = twin bands, *G* = growth striations, *L* = line contrasts.

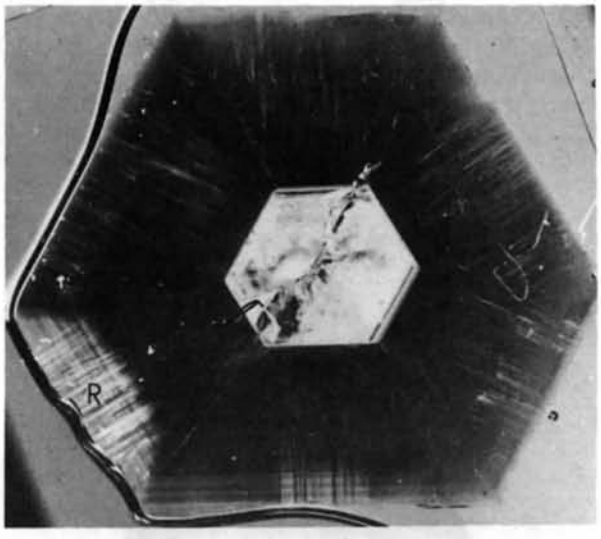

(*a*)

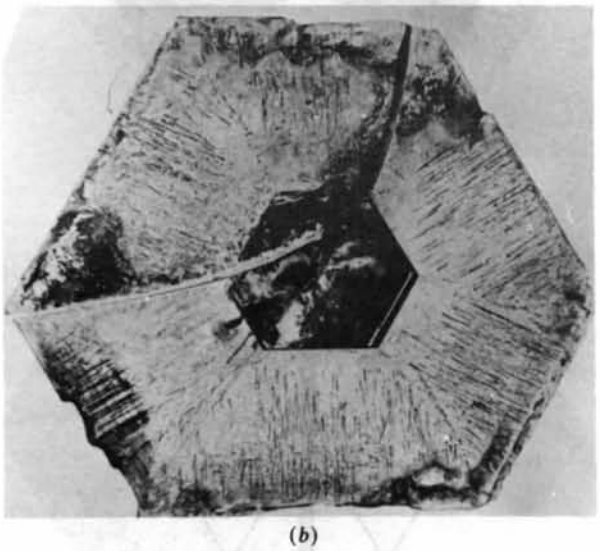

(*b*)

Fig. 8. Plate parallel to (0001) cut above the seed crystal. Thickness ≃1 mm, horizontal dimension 12 mm. (*a*) optical photograph of the plate between polarizers deviating by 3° from the crossed position. Inner bright region: (0001) growth sector. Region *R* of higher brightness has grown on a prism face, the other parts of the plate have grown on pyramid faces. (*b*) Pyroelectric decoration pattern. Only one side is decorated.

nature of these striations is not yet clear. Investigations with methods of higher resolution like electron microscopy might be helpful.

X-ray topographs of the plates of Figs. 7 and 8 are given in Fig. 9. Some line contrasts in Figs. 7 and 8 are also visible in the topographs. The growth striations S are not revealed by X-ray topography.

3.2. *Dislocations*

The grown-in dislocations show an arrangement typical for solution growth. They originate from inclusions at the seed surface and from other growth defects and proceed as straight lines with rather well defined directions which depend on the Burgers vector and the growth direction. Burgers vectors parallel to ⟨100⟩ and, less frequently, [001] have been identified. At the intersection with a growth-sector boundary, which is in many cases also a twin interface, a sharp bend of the dislocation line occurs (Figs. 3*a* and 3*b*). No change in the direction of dislocation lines is observed at twin boundaries like *O*–*O* in Fig. 3. This is in agreement with the minimum-energy theory of preferred dislocation-line directions (Klapper & Küppers, 1973), because the elastic properties and the growth direction are not changed across the $m_{\parallel}$-twin boundary *O*–*O*.

The dislocation arrangement is different in the various growth sectors. In the *basal* sectors {0001} the dislocations are always parallel to [001] and have pure screw or pure edge character (Figs. 3*a* and 3*b*). In the *prism* regions $\{10\bar{1}0\}$ all dislocations are parallel to (0001). The majority are either parallel to the growth direction ⟨210⟩ (mainly edge character) or close to the ⟨100⟩ directions with predominant screw character (Fig. 9*a*). In the *pyramid* growth sectors $\{\bar{1}0\bar{1}0\}$ two groups of dislocation lines dominate. One group consists of dislocation lines parallel to (0001) with directions close to their Burgers vector along ⟨100⟩. The other group contains dislocations with directions closely parallel to the growth normal. They have either edge character with Burgers vector parallel to one of the three ⟨100⟩ directions or they are mixed with Burgers vector along [001].

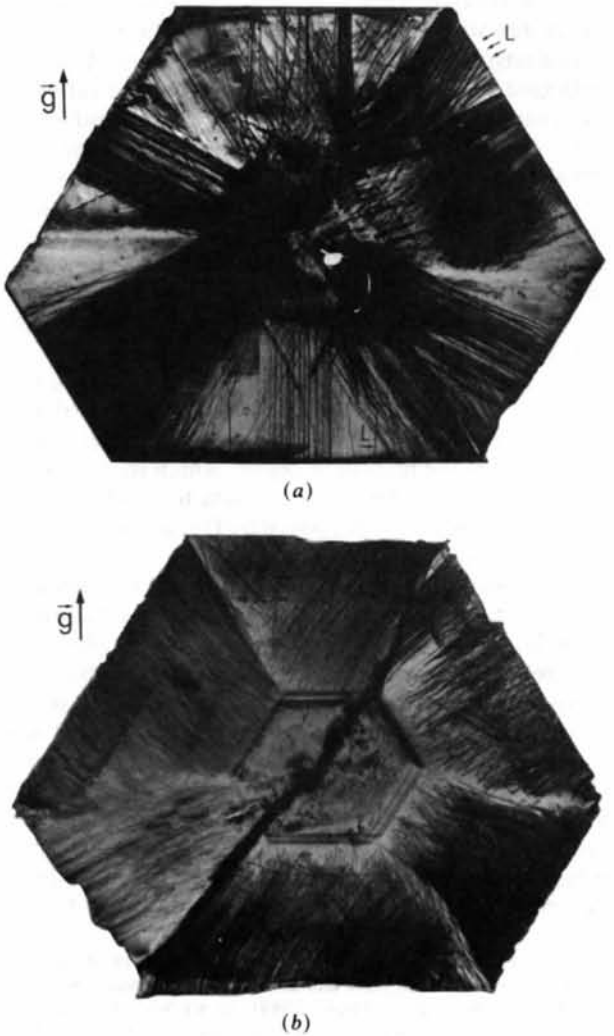

Fig. 9. Arrangement of dislocations in the two plates (*a*) and (*b*) of Figs. 7 and 8. X-ray topographs in reflection $30\bar{3}0$.

4. Discussion

4.1. *Relation to crystal growth*

The main features of twinning in $KLiSO_4$ may be summarized as follows:

(*a*) In the prism and, less frequently, in the pyramid sectors numerous thin twin lamellae parallel to (0001) with twin law $m_{\parallel}$ occur. They originate from growth defects (*e.g.* inclusions). The density of the lamellae is often too high to be resolved by X-ray topography. Boundaries parallel to (0001) with an inversion of the electrical axis ($m_{\perp}$ or $2_{\perp}$) are rarely found.

(*b*) In many specimens isolated large twin boundaries $m_{\parallel}$ exactly parallel to (0001) extend through the whole crystal. In a few cases these boundaries coincide with the (0001) facets of the seed crystals.

(*c*) Frequently, boundaries between different growth sectors separate regions of opposite electric polarity according to twin law $m_{\perp}$ ('growth-sector twins').

(*d*) Growth sectors (0001) are free of type II twinning.

For the understanding of the observed geometry and distribution of twin domains in $KLiSO_4$ the following crystal-growth processes must be considered: (i) nucleation of twin domains, and (ii) advance of a twin boundary with the growing crystal.

Nucleation of twin domains. Twinning in $KLiSO_4$ is nucleated by crystal defects. This is clearly visible for the twin lamellae which originate from liquid

inclusions in the pyramid sectors and at the surface of the seed crystals. Obviously, the nucleation energy of a twin domain on an undisturbed growth face is too high to allow appreciable twin formation. Presence of inclusions which cause strong distortions of the surrounding crystal matrix, however, increases the probability of twin nucleation. Twinning is thus closely correlated with the perfection of the crystal, which is dependent on the growth conditions. The high density of twin lamellae in the prism sectors grown on prism seed plates (Fig. 6) is a result of the highly disturbed growth zone at the surface of the seed plate. Furthermore, there is a strong dependence of twin nucleation on the growth face. No twins are formed in the (0001) sectors (Figs. 2 and 5) although enough inclusions at the {0001} surfaces of the seed crystals are present which could act as nucleation centres.

Propagation of twin boundaries during growth. A twin boundary or a twin lamella, once nucleated, proceeds with the growing crystal and forms an interface with minimal boundary energy. It is obvious that the boundary orientation actually realized depends on the twin law and on the growth sector in which the interface is located. Typical examples are the $m_{\parallel}$ boundary O-O and the growth-sector twin boundaries W_1, W_2 in Figs. 2 and 3. Although all three boundaries start from a (0001) seed facet, they follow quite different surfaces.

For topological reasons a single twin boundary cannot abruptly terminate during growth. A twin lamella emerging from a growth face, however, may be closed off by succeeding growth layers. Closed-off twin lamellae were not observed in $KLiSO_4$.* This demonstrates that it is energetically more favourable for a twin lamella to proceed with the growing crystal.

4.2. *Structural models of twin boundaries*

Although no quantitative values of the boundary energy can be given, qualitative considerations may help one to understand the geometry of twin boundaries. The boundary energy depends on the degree of distortion of the crystal structure in the contact region. If a model of the twin interface with minimal deformation of the crystal structure can be devised, it can be assumed that the twin boundary is of low energy and that it occurs frequently.

It is well known that low-energy interfaces are often simple crystallographic planes. Examples are Brasil twin boundaries in quartz (McLaren & Phakey, 1966, 1969) or domain boundaries in ferroelectrics (*cf.* Känzig, 1957).

The following models of twin boundaries in $KLiSO_4$ are derived from the assumption that the linking of the tetrahedral framework continues across the twin interface, and that direct links of two SO_4 or two LiO_4 tetrahedra are forbidden.* Two types of structural distortions occur in these models:

(i) The frameworks of the two twin partners can be linked across the contact plane without misfit of the tetrahedral apices. In this case the lattice suffers no deformation but changes of orientation of tetrahedra and of coordination of potassium may occur. This type of boundary is considered to be of low energy.

(ii) Only part of the tetrahedra can be linked across the contact plane without misfit whereas the other apices do not match. A measure of this mismatch may be given by the 'linking-misfit vector' $\mathbf{q}$ connecting the separated apices. Joining of these corners leads to a lattice deformation. In addition, the structural changes mentioned in (i) may occur. This type of boundary is considered to be of higher energy.

At first, models of twin interfaces with twin law $m_{\parallel}$ are considered. This law relates enantiomorphous structures with the same direction of the polar axis. Comparison of Figs. 10(*a*) and 10(*b*) shows that one structure variant can be obtained from the other by rotation of the tetrahedra by nearly 60° around [001], whereby the sense of rotation of the SO_4 and the LiO_4 tetrahedra is opposite. In Fig. 11(*a*) the two structure variants are connected across the composition plane (0001). It is obvious that the structure continues without misfit [case (i)]. In the interface, however, the tetrahedra are eclipsed in contrast to the staggered orientation in the interior of the domains. The coordination number of the K ions remains 9.

For the composition plane $(10\bar{1}0)$ a linking misfit vector $\mathbf{q} \neq 0$ results (Fig. 11*c*). The removal of this misfit by the joining of apices leads to a rather strong distortion of the transition region which increases the coordination number of potassium to 11 (Fig. 11*b*). The same model was proposed by Dollase & Freeborn (1977) for $KAlSiO_4$.

Other suitable boundaries could not be deduced for twin law $m_{\parallel}$. Comparison of the two boundary models above shows that contact plane (0001) is energetically favoured. This is actually observed. Large-area twin boundaries and twin lamellae parallel to (0001) occur with high frequency (*cf.* Figs. 2 and 3), whereas large $(10\bar{1}0)$ boundaries are not observed.

According to the structural model of Fig. 11(*a*) no long-range lattice distortions should be present near the (0001) boundaries. Although X-ray topography is highly sensitive to small distortions, the absence of deformations could not be observed owing to the

* Twin lamellae, however, were observed to terminate at inclusions.

* It should be noted that the tetrahedral framework of quartz is not interrupted by Dauphiné and Brasil twin boundaries (McLaren & Phakey, 1966, 1969; Phakey, 1969). In $KLiSO_4$, however, the framework is less strong owing to the weaker Li-O bonds. Thus, boundaries with a break of the framework may be more easily realized than in quartz.

abundance of other distortions (*cf.* Fig. 3). For the same reason dynamical contrasts could not be observed, *i.e.* the zero fault vector proposed by the model could not be confirmed.

Next, twin laws $m_\perp$ and $2_\perp$ are considered. They involve a reversal of the polar axis. Here all those composition planes which are inclined to [001] should be electrically charged. Boundaries of this type have a high electrostatic energy and are therefore highly improbable. This is the reason why in ferroelectrics 180° 'head-to-head' or 'tail-to-tail' boundaries normally do not occur. They can be formed if the crystal is electrically conducting, which allows the boundary charges to be cancelled out (Little, 1955).

Boundaries parallel to [001] are uncharged. Of these, reasonable models could be derived only for contact plane $(10\bar{1}0)$. The models are shown in Figs. 12(*a*) and 12(*b*) and can be characterized as follows:

(i) Both models contain four-membered rings of tetrahedra across the contact plane. This implies a considerable distortion of the structure in both cases.

(ii) The model for twin law $m_\perp$ has no linking misfit ($\mathbf{q}=0$), whereas for $2_\perp$ the same misfit vector occurs as in $m_\parallel$ (Fig. 11*c*). This makes $m_\perp$ more favourable than $2_\perp$.

(iii) The coordination number 9 of the K ions in the interior of the domains changes in the boundary plane to 8 and 10 for twin law $m_\perp$ and to 10 and 12 for $2_\perp$.

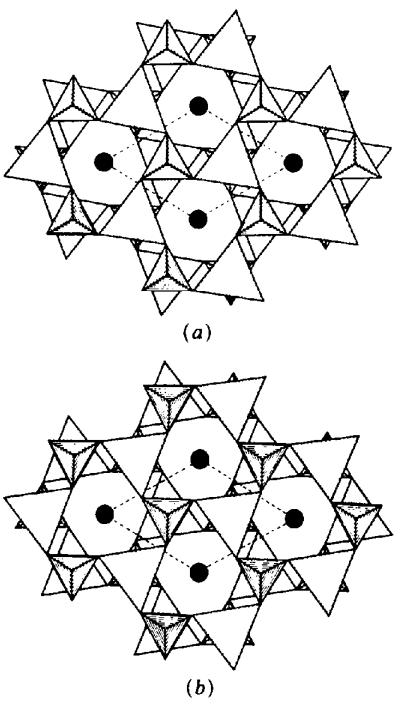

Fig. 10. Enantiomorphous structures of $KLiSO_4$, related by the mirror plane $m_\parallel$. View along [001]. Small tetrahedra: SO_4 groups, large tetrahedra: LiO_4 groups, full circles: potassium ions. The unit cell is indicated by dashed lines.

It is surprising that in $KLiSO_4$ no boundaries parallel to the electric axis are found, either for twin law $m_\perp$ or for $2_\perp$. The only possible exception is the $m_\perp$-twinning associated with the $\{10\bar{1}0\}$ growth striations in Fig. 7(*a*). Actually observed, however, are two kinds of 'electrostatically forbidden' 180° boundaries, both inclined to [001].

Twin boundaries of the first kind always have twin law $m_\perp$ and coincide with growth-sector boundaries. They follow an irregular course and their inclination towards [001] varies between parallel and perpendicular orientations. It is obvious from Figs. 2(*a*) and

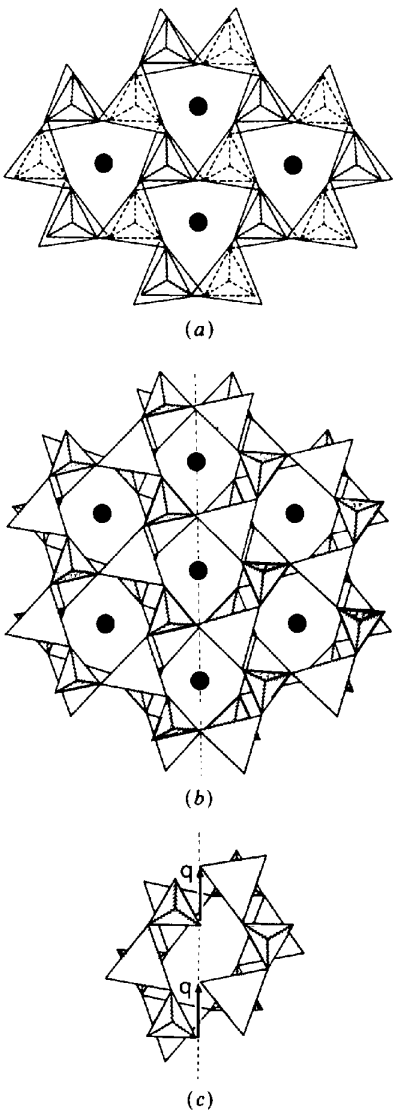

Fig. 11. Structural models of twin boundaries for twin law $m_\parallel$ in $KLiSO_4$. (*a*) Boundary parallel to (0001). The twin interface lies between the two tetrahedral layers. (*b*) Boundary (dashed line) parallel to $(10\bar{1}0)$. (*c*) Misfit of the undistorted $m_\parallel$-twin partners across the $(10\bar{1}0)$ boundary. Only one pair of six-membered rings is shown. The tetrahedral layer (in this drawing the bottom layer) can extend across the interface without misfit. In the next (top) layer a linking-misfit vector $\mathbf{q}$ occurs.

4 that these antipolar domains have been nucleated independently on different seed facets and forced to arrange themselves during growth along an electrostatically unfavourable boundary. Since the crystal grows in an electrolytic solution, this adaptation is facilitated by the presence of positive and negative ions which neutralize the boundary charges and reduce the electrostatic energy. It would be meaningless to devise structural models for these irregular boundaries. The framework is probably interrupted and the twin interface consists of a highly disordered, possibly nonstoichiometric layer.

Similar considerations apply to the structure of the second kind of unfavourable boundaries ($m_\perp$ or $2_\perp$) which always have (0001) orientation and occur in the prism sectors. Such boundaries are present in the densely twinned regions in Figs. 2 and 3 and in Fig. 6. They must involve a poor structural fit because they are accompanied by appreciable distortions of the crystal. This is demonstrated by strong kinematical X-ray contrast and by the presence of etch grooves.

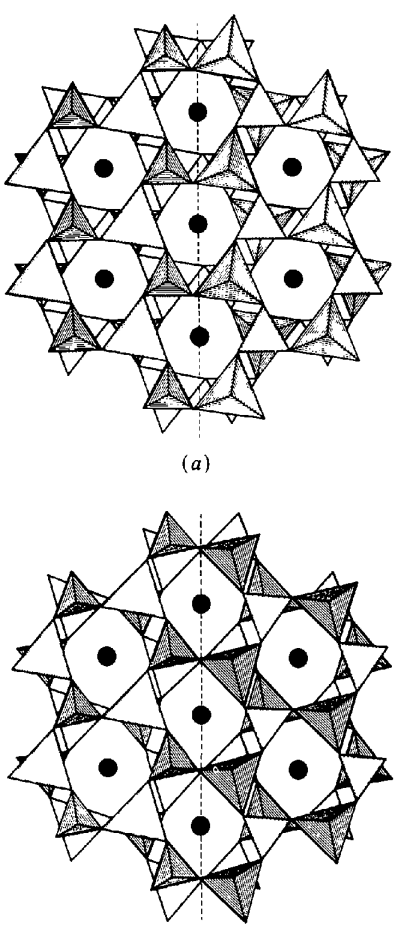

Fig. 12. Structural models of $(10\bar{1}0)$ twin boundaries (dashed lines) with reversal of the electric axis. (*a*) Twin law $m_\perp$. No distortion of the tetrahedral framework in the neighbourhood of the contact plane ('misfit vector' $\mathbf{q} = 0$). (*b*) Twin law $2_\perp$. Distorted transition region as in Fig. 11(*b*).

It must be concluded that the occurrence of the electrically unfavourable boundaries is due to independent nucleation of antipolar domains. No explanation, however, can be advanced for the absence of the electrically favourable contact planes for which two reasonable models could be devised which, however, require considerable changes in the coordination of atoms and distortions of the framework. This demonstrates the great difficulties of structural interpretations of twin boundaries.

In contrast, the absence of $m_\parallel$-twinning in the (0001) growth sectors can be explained. This twinning occurs with high abundance in the prism and pyramid sectors. As shown above, for $m_\parallel$ twins only the (0001) interface has low energy. This twin boundary, however, becomes unfavourable if it is formed on the (0001) growth face. Since growth proceeds layer by layer, the whole energy of the large-area (0001) boundary has to be provided within the growth period of one layer. This is highly improbable even for the structurally favoured (0001) interface of $m_\parallel$ twins.

5. Concluding remarks

In $KLiSO_4$ three possible twin laws and four domain variants are predicted by the subgroup–supergroup relations between point group 6 and holohedry $6/mmm$. They were all found to occur in one and the same crystal. Only by combination of the three methods, optical activity, pyroelectric decoration and X-ray topography, applied to large crystals grown from aqueous solution, could a comprehensive characterization and description of the twinning and the twin domains in relation to crystal growth and crystal perfection be obtained.

The essential results of this investigation are:

(i) A strong dependence of the twin laws present and of the shape and arrangements of the twin domains on the growth sector exists. Certain growth sectors are always twin-free, thus yielding untwinned specimens for accurate structure determination and inelastic neutron scattering.

(ii) Twin domains are nucleated at growth defects, mainly at inclusions and at the surface of the seed crystal. The density of twin domains is therefore strongly influenced by the crystal perfection and, indirectly, by the growth conditions.

(iii) The occurrence of 'growth-sector (inversion) twins' leads to 'electrically forbidden' head-to-head and tail-to-tail twin boundaries. This can only be understood on the basis of growth from electrolytic solution.

(iv) The frequently observed large-area (0001) boundaries between enantiomorphic domains of equal polarity are of low energy, as is revealed by structural models of twin interfaces.

We are indebted to the Deutsche Forschungsgemeinschaft for support of this work.

References

ABELLO, L. (1985). *J. Chem. Thermodyn.* **17**, 1023-1025.

BALAGUROV, A. M., SAVENKO, B. N., DLOUHA, M., VRATISLAW, S. & JIRAK, Z. (1984). *Phys. Status Solidi A*, **83**, K117-K121.

BANSAL, M. L. & ROY, A. P. (1984). *Phys. Rev.* **30**, 7307-7309.

BHAKAY-TAMHANE, S., SEQUEIRA, A. & CHIDAMBARAM, R. (1985*a*). *Acta Cryst.* C**40**, 1648-1651.

BHAKAY-TAMHANE, S., SEQUEIRA, A. & CHIDAMBARAM, R. (1985*b*). *Solid State Commun.* **53**, 197-200.

BLITTERSDORF, H. (1929). *Z. Kristallogr.* **71**, 141-168.

BORN, M. (1933). *Optik*, pp. 413-420.

BRADLEY, A. J. (1925). *Philos. Mag.* **49**, 1225-1237.

BUERGER, M. J. (1954). *Am. Mineral.* **45**, 600-614.

BURY, P. C. & MCLAREN, A. C. (1969). *Phys. Status Solidi*, **31**, 799-806.

CACH, R., TOMASZEWSKI, P., BASTIE, P. & BORNAREL, J. (1984). *Ferroelectrics*, **53**, 337-340.

CACH, R., TOMASZEWSKI, P. & BORNAREL, J. (1985). *J. Phys. C*, **18**, 915-923.

CATTI, M. & FERRARIS, G. (1976). *Acta Cryst.* A**32**, 163-165.

CHUNG, S. J. (1972). *Tetraedergerüste bei Fluoberyllaten und Sulfaten.* PhD Thesis, Technische Hochschule, Aachen.

CHUNG, S. J. & HAHN, TH. (1972*a*). *Acta Cryst.* A**28**, S57-S58.

CHUNG, S. J. & HAHN, TH. (1972*b*). *Mater. Res. Bull.* **7**, 1209-1218.

DOLLASE, W. A. & FREEBORN, W. P. (1977). *Am. Mineral.* **62**, 336-340.

DONNAY, G. & DONNAY, J. D. H. (1974). *Can. Mineral.* **12**, 422-425.

ECKOLD, G. & HAHN, TH. (1987). In preparation.

FONSECA, C. H. A., RIBEIRO, G. M., GAZZINELLI, R. & CHAVES, A. S. (1983). *Solid State. Commun.* **46**, 221-225.

FUJIMOTO, S., YASUDA, N. & HIBINO, H. (1984). *Phys. Lett.* **104A**, 42-43.

FUJIMOTO, S., YASUDA, N. & HIBINO, H. (1985*a*). *J. Phys. D*, **18**, L135-L137.

FUJIMOTO, S., YASUDA, N. & HIBINO, H. (1985*b*). *J. Phys. D*, **18**, 1871-1882.

HAHN, TH. (1981). *Z. Kristallogr.* **156**, 114-115.

HAHN, TH. & CHUNG, S. J. (1973). *Z. Kristallogr.* **137**, 447-449.

HAHN, TH., LOHRE, G. & CHUNG, S. J. (1969). *Naturwissenschaften*, **56**, 459.

HAHN, TH., LOHRE, G. & CHUNG, S. J. (1970). *Z. Kristallogr.* **132**, 431.

IVANOV, N. R. (1985). *Ferroelectrics*, **64**, 13-18.

KÄNZIG, W. (1957). *Ferroelectrics and Antiferroelectrics.* London: Academic Press.

KARPPINEN, M., LUNDGREN, J. O. & LIMINGA, R. (1983). *Acta Cryst.* C**39**, 34-38.

KASSEM, M. E., EL-WAHIDY, E. F., KANDIL, S. H. & EL-GAMAL, M. A. (1984). *J. Therm. Anal.* **29**, 325-331.

KLAPPER, H. & KÜPPERS, H. (1973). *Acta Cryst.* A**29**, 495-503.

KRAJEWSKI, T., BRECZEWSKI, T., KASSEM, M. & MRÓZ, B. (1984). *Ferroelectrics*, **55**, 143-146.

KRAJEWSKI, T., BRECZEWSKI, T., PISKANOWICZ, P. & MRÓZ, B. (1985). *Ferroelectrics Lett.* 4, pp. 95-99.

KUNDT, A. (1883). *Ann. Phys.* **20**, 592-603.

LANG, A. R. (1959). *J. Appl. Phys.* **30**, 1748-1755.

LANG, A. R. (1965). *Appl. Phys. Lett.* **7**, 168-170.

LANG, A. R. (1967). *Crystal Growth*, edited by H. S. PEISER, pp. 833-838. Oxford: Pergamon. (Suppl. No. 1 to *J. Phys. Chem. Solids.*)

LI, Y. Y. (1984). *Solid State Commun.* **51**, 355-358.

LITTLE, E. A. (1955). *Phys. Rev.* **98**, 978-984.

MCLAREN, A. C. & PHAKEY, P. P. (1966). *Phys. Status Solidi*, **13**, 413-422.

MCLAREN, A. C. & PHAKEY, P. P. (1969). *Phys. Status Solidi*, **31**, 723-737.

MAEZAWA, K., TAKEUCHI, H. & OHI, K. (1985). *J. Phys. Soc. Jpn*, **54**, 3106-3110.

NACKEN, R. (1907). *Neues Jahrb. Mineral. Beil. Bd*, **24**, 42-52.

PHAKEY, P. P. (1969). *Phys. Status Solidi*, **34**, 105-119.

SANDOMIRSKII, P. A., MESHALKIN, S. S. & ROZHDESTVENSKAYA, I. V. (1983). *Sov. Phys. Crystallogr.* **28**, 33-35.

SCHULZ, H., ZUCKER, U. & FRECH, R. (1985). *Acta Cryst.* B**41**, 21-26.

SCIVESSY, G. (1928). *Handbuch der Physik*, Vol. 20, edited by H. GEIGER & K. SCHEEL, pp. 804-837. Berlin: Springer.

TOMASZEWSKI, P. E. & LUKASZIEWICZ, K. (1983). *Phase Transition*, **4**, 37-45.

TRAUBE, H. (1892). *Neues Jahr. Mineral. Geol.* **II**, 58-67.

TRAUBE, H. (1894). *Neues Jahrb. Mineral. Geol.* **I**, 171-184.

WYROUBOFF, G. (1890). *Bull. Soc. Fr. Mineral.* **13**, 215-233.

YOUNG, P. W., KATIYAR, R. S. & SCOTT, J. F. (1984). *J. Raman Spectrosc.* **15**, 347-349.

ZEKS, B., LAVRENCIC, B. & BLINC, R. (1984). *Phys. Status Solidi B*, **122**, 399-404.